# Extensional flow-based assessment of red blood cell deformability using hyperbolic converging microchannel

**Sung S. Lee · Yoonjae Yim · Kyung H. Ahn ·
Seung J. Lee**

**Abstract** The deformability of the red blood cell (RBC), is known to be closely related to microcirculation and diagnosis of specific diseases such as malaria, arterial sclerosis, sepsis, and so on. From the viewpoint of the flow type, conventional methods to measure the cell deformability have exploited simple shear or complex flow field with little focus on extensional flow field. In this paper, we present a new approach to assess cell deformability under the extensional flow field. For this purpose, a hyperbolic converging microchannel was designed, and the cell deformation in the extensional flow region was continuously monitored. It overcomes the limitation of conventional methods by reducing experiment time. As quantified by the degree of deformation, the extensional flow (Deformation Index = 0.51 at 3.0 Pa) was found to be more efficient in inducing cell deformation compared to the shear flow (Deformation Index = 0.29 at 3.0 Pa). This indicates the insufficiency of the existing models that predict the blood damage in artificial organs, which only consider shear flow. Also, this method could detect the heat-induced difference in deformability of RBCs. It provides a new platform to study the clinical effect of RBC deformability under extensional flow, and is expected to contribute the association of several diseases and deformability of RBCs.

**Keywords** Deformability · Extensional flow ·
Hyperbolic converging channel · Microfluidic device

S. S. Lee · Y. Yim · K. H. Ahn (✉) · S. J. Lee
School of Chemical and Biological Engineering,
Seoul National University,
Shillim-dong,
Gwanak-gu, Seoul 151-744, Korea
e-mail: ahnnet@snu.ac.kr

## 1 Introduction

There is a growing interest in microfluidic devices as a tool for clinical and biological application. One of the key issues in this area is to invent a blood analysis device such as blood typing (Kim et al. 2006) and plasma separation (Delinder and Groisman 2006; Yang et al. 2006) for a point-of-care (POC) diagnostic system. The red blood cell (RBC), the major component of blood, contains a lot of physiological and clinical information. Among the information, the RBC deformability is known to be an important physical property in the delivery of oxygen to the tissues. In order to supply the tissues with oxygen, normal RBCs (mean diameter = 7 μm) should pass through capillary vessels, whose diameter is much smaller than their mean diameter. A decrease in deformability evokes an impaired perfusion of the peripheral tissues (Simchon et al. 1987) and contributes to splenic clearance of infected RBCs, since the cells must squeeze through small intercellular gaps in the spleen. This is one of the mechanisms by which the spleen removes the aged RBCs (Suwanarusk et al. 2004). Thus the assessment of deformability is expected to be associated with the diagnosis or prediction of specific diseases related to RBC physical properties (Mokken et al. 1992).

Since the importance of deformability has became apparent, it has been measured by various experimental methods (Couette device: Dobbe et al. 2002; Micropippet: Evans 1983; Paulitschke and Nash 1993, Optical tweezers: Dao et al. 2003). From the viewpoint of the flow type (Fig. 1), these conventional methods do not seriously consider the response of the cells under the extensional flow field. The Couette device induces the deformation of RBCs under simple shear flow by the drag force acting on the fluid between two surfaces. Though optical tweezers and micropipet are known to give some extensional
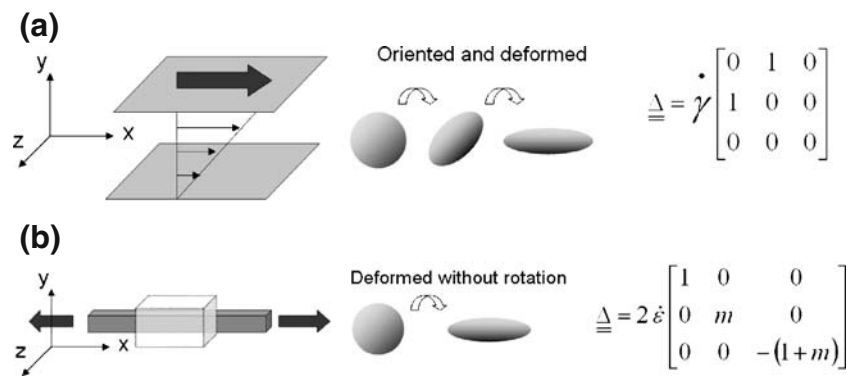
properties, those methods cannot avoid direct contact with the cell surfaces, and require time-consuming experiments.

It is necessary to understand the response of RBCs under the extensional flow field. Firstly, there are many locations where the extensional flow dominates either in the blood flow, or the flow in the extracorporeal devices. Extensional flow is caused at a region of contraction by the velocity difference between before (wider and lower velocity) and after (narrower and higher velocity) the contraction. For example, when RBCs pass through a junction between a wide vessel and a narrow catheter or phlebotomy needles, they experience extremely high extensional flow and should be broken up (Sharp and Mohammad 1998; Umezu 1994; Grant 2003). The breakup of the cell is called hemolysis, which often becomes a fatal problem in the development of artificial organs because the residue of broken cells initiates coagulation and blocks the vessel. Secondly, it can complement the limitation of conventional approaches to deformation of RBC, which are based only on measurement under simple shear flow. Essentially, complex flow can be regarded as a combination of shear and extensional flow from the kinematic view, so it is necessary to estimate the deformation not only under shear flow, but also under extensional flow. Furthermore, it is expected to give an insight into improving the model predicintg hemolysis in artificial organs, since the degree of deformation has recently been correlated with hemolysis (Arora et al. 2004)

In this paper, we present a new approach to assess RBC deformability by investigating extensional flow-induced deformation using a hyperbolic converging microchannel and optical image enhancement (Figs. 2 and 3).

## 2 Experimental section

### 2.1 Materials

Blood taken from an adult rabbit was put into K3-EDTA vacuum tube right after withdrawal to avoid RBC coagulation.

The whole blood was suspended in polyvinylpyrolidone (PVP) solution (6.8 wt% and 12 wt%) to control the applied fluidic stress level to cells. To balance pH and osmotic pressure, PVP was dissolved in phosphate buffered saline solution (PBS: 0.01 M phosphate buffer, 0.0027 M potassium chloride and 0.0137 M sodium chloride; pH 7.4, osmotic pressure 290 mOsm/kg, Sigma Chemical Co.). The volume ratio of blood to PVP solution (RBC/PVP) was 0.001 L/L in 10.0 mL of the PVP solution. The shear viscosity of PVP solution was measured by a rheometer (Bohlin, C-VOR).

### 2.2 Microfluidic device

We designed the hyperbolic converging microchannel to induce the extensional flow in the converging region as shown in Fig. 2(a). The width of the sidewalls contracts from 2,000 μm ($L_w$) to 200 μm ($L_n$) along a hyperbolic equation [ $h(x) = \frac{1}{\frac{2}{Lc}\left(\frac{1}{Ln}-\frac{1}{Lw}\right)x+\frac{2}{Lw}} = \frac{1}{Ax+B}$, $L_w$, $L_n$, $L_c$ : wide and narrow dimension of converging channel, and length of converged region, $L_w=2,000$ μm, $L_n=200$ μm, $L_c = 3,000$ μm, $A=-3.0\times10^{-5}$ μm$^{-2}$, $B=1\times10^{-3}$ μm$^{-1}$, unit of $x$ is μm and ($x=0$: at the beginning of converging region) ]. In a hyperbolic converging channel, the total Hencky strain along the centerline of the channel is determined by the ratio of wide to narrow dimension of the converging channel as $\varepsilon_H = \ln(L_w / L_n)$ (Feigl et al. 2003). Although, here, we showed the experimental result with a ratio of the condition ($L_w / L_n = 10$), the effect of total strain on RBCs can be investigated by controlling the ratio of ($L_w / L_n$).

The Microchannel was made by molding polydimethylsiloxane (PDMS, Sylgard 184, Dow) upon a silicon wafer containing a positive-relief channels pattern of SU-8 photoresist (height=75 μm). (Xia and Whitesides 1998). The microchannel was carefully peeled off and attached to PDMS coated slide glass, so that the microfluidic device was formed with four PDMS-walled channels. The plasma sterilizer (PDC-32G, Harrick) was used to attach them. After plasma treatment, we placed the microfluidic device in an oven at 135°C for 72 h to increase bonding strength.
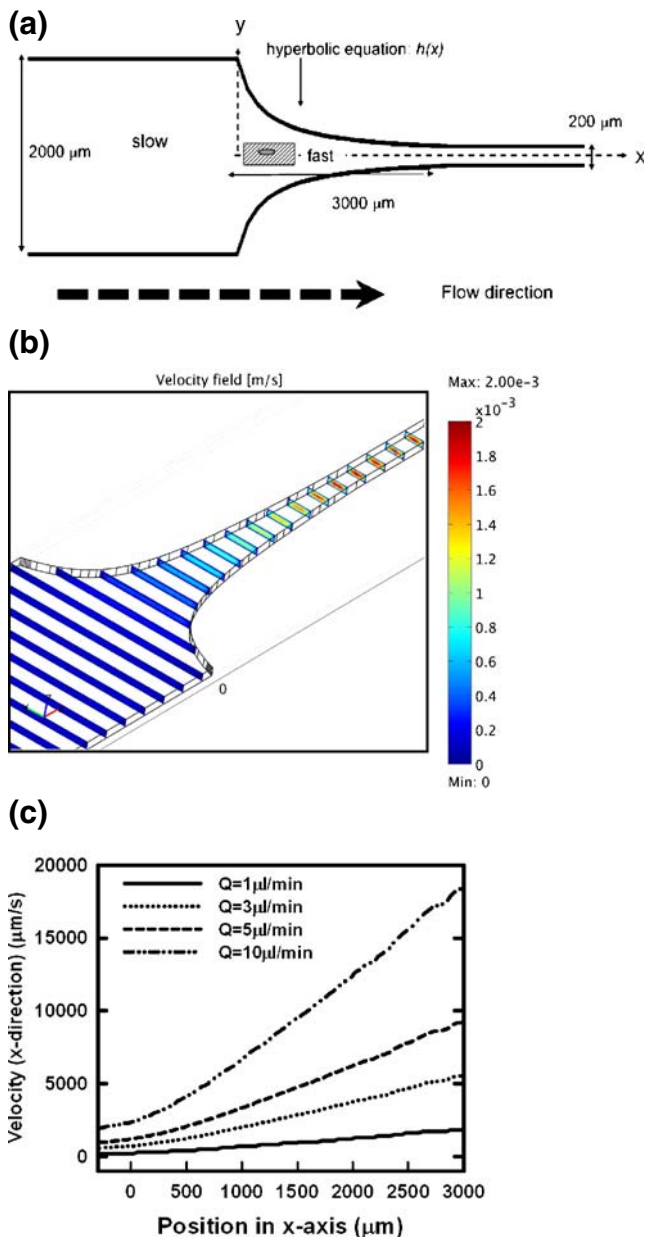
**Fig. 2** Hyperbolic converging microfluidic channel (**a**) Design; the extensional flow induced by velocity difference along the x axis in hyperbolic converging region. Red blood cells (RBCs) deform when they pass through the converging region. (**b**) Velocity field, flow rate Q=1 μl /min (**c**) Velocity of x-axis direction at the centerline of channel. The slope of this graph implies the extensional rate

## 2.3 RBC deformability measurements

Images of RBCs were enhanced by a small bandwidth interference filter (380–420 nm). The light absorption coefficient in the Soret region (415 nm, violet) is relatively high for hemoglobin of RBCs. The RBCs appear as dark objects against a bright background in the region of the spectrum (380–420 nm) so that it is easy to detect the edge of the focused cell very clearly (Fig. 3). Without a filter, it

was difficult to define the edge of the cells. The enhanced images were taken by camera and analyzed easily.

For simple shear flow, we used a Couette device (CSS 450, Linkam) mounted on a microscope (BX 51, Olympus). We introduced 0.5 mL of sample between two rotating glass disks of the CSS 450 shearing cell, illuminated with optically filtered (380–420 nm) white light, and observed by CCD camera (HR 50, Sony). The speed of the rotating plate was incrementally raised to increase the shear stress level. At each shear level, 500 images were successively captured and analyzed.

For extensional flow field, the microfluidic device was used and was mounted on an inverted microscope (IX 71, Olympus). We input the RBC/PVP suspension by use of a digitally operated syringe pump (KDS 210, Kdscientific) through PTFE tubing. The extensional rate was controlled by the input flow rate. Practically, it was difficult to control the low flow rate stably (less than 0.5 μl /min) due to the fluctuation phenomenon of syringe pump. Thus, for low extensional stress (<0.5 Pa) conditions, we used low viscosity ($\eta_e$=0.093 Pa s) of PVP (6.8%) and higher flow rate. Other extensional stress experiments were performed with 12% of PVP solution ($\eta_e$=0.89 Pa s). At each flow rate, we carefully focused the middle of the channel at a region of interest (ROI), and 500 images were successively captured by high-speed camera (ultima 512, Photron). RBCs in ROI were analyzed, and their degrees of deformation were quantified. The extensional viscosity ($\eta_e$) was considered as three times that of shear flow ($\eta_s$) [$\eta_e= 3\eta_s$.] by Trouton's rule (Trouton 1906)
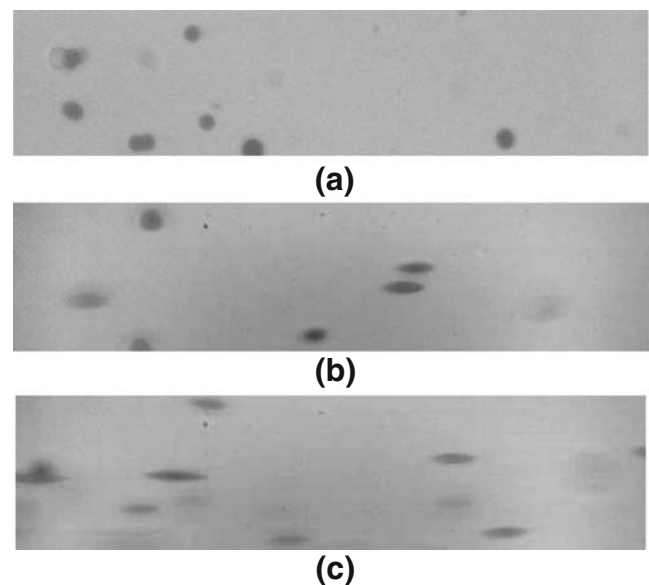


**Fig. 3** Typical images of deformed RBCs under extensional flow; (**a**) without flow, (**b**) extensional stress = 3.0 Pa, and (**c**) extensional stress= 9.0 Pa; flow direction from left (slower region) to right (faster region)

The acquisition rate is carefully chosen to prevent including the same cells in next image. The flowing distance of cells until the next image is taken (it takes time as inverse of acquisition rate) must be larger than the major length of the FOV (field of view by camera). The major length of FOV was 120 µm since it was performed with a 40× objective lens and a 1/3″ CCD camera. For example, if the sample is inputted with Volume Flow Rate: Q=10 µl /min, we recommend the acquisition rate should be lower than 1,111 µm s$^{-1}$/120 µm≈10 Hz because average linear velocity at inlet (before the hyperbolic converging region) is calculated as 1,111 µm/s (average linear velocity = (Volume Flow Rate) / (Cross section Area): v = Q/A = (10 µl/min) / (2,000 µm×75 µm). In order to increase the percentage of RBCs analyzed through the ROI over the total number of cells, a higher acquisition rate is better as long as the same cells are not including in the next images. The exposure time for each image was chosen as less than 1/10,000 sec).

The images of deformed RBCs were analyzed by open software (ImageJ, NIH). The degree of RBC deformation was quantified by the Deformation Index (DI) defined as $DI = \frac{X-Y}{X+Y}$, where X and Y are the major and minor lengths of the deformed cell. The major and minor lengths were found by fitting to an ellipsoid shape. Aggregated or overlapped RBCs were excluded from the analysis by considering the size of area (>150 µm$^2$) (Dobbe et al. 2002).

# 3 Results and discussion

## 3.1 RBC deformation under extensional flow

We observed the RBC deformation under constant extensional flow. The deformation is induced via a microfluidic converging channel (Fig. 2(a)). The converging channel generates the extensional flow by the difference in velocity between wide and narrow channels. It is known that a constant extensional rate can be generated over a wide range of converging regions if the shape of converging channel follows the hyperbolic function (Feigl et al. 2003; Mobuchon et al. 2005; Randall et al. 2006).

To obtain the value of the constant extensional rate in a hyperbolic converging region, a 3D numerical simulation (number of mesh element: 107,444) was conducted using a commercial package (Fluent) (Fig. 2(b) and (c)). The incompressible Navior-stokes equation option was chosen for numerical simulation, and input flow rates were tuned for the calculation of extensional rate in each experimental condition. The computational flow field differed from a classical Poiseuille flow (flow in straight pipe) within a converging channel (Fig. 2(b)). The velocity of x-axis direction at the centerline of the channel increases linearly

(Fig. 2(b)). It implies that the extensional rate is constant in the converging region, which is defined as the rate of velocity. In the case of the classical Poiseuille flow, the extensional rate is zero, since the velocity is constant along the centerline of the channel. In this study, the experimental input flow rates were controlled from 0.5 µl/min to 100 µl/min, and the extensional rate obtained numerically were from 0.28 s$^{-1}$ to 56.2 s$^{-1}$, respectively. From this numerical calculation and the correlation: *Applied extensional stress = Extensional viscosity × Extensional rate,* we could determine the adequate input flow rate for applied extensional stress [e.g. 0.9 (Pa)=0.89 (Pa s)×1.01 (s$^{-1}$) by operating input flow rate=1.8 µl/min]

The region of interest (ROI) was carefully chosen. Firstly, the position of ROI in the x-axis was chosen in the middle of the hyperbolic converging region as (x= 1,200 µm) because at this position, the extensional flow rate is constant on the basis of the numerical simulation, and if the position is near to the end of converging region, the velocity can be so fast as to surpass the shutter speed of camera. The size of the ROI (120 µm×20 µm) was chosen as smaller than the actual cross section of the channel. One hundred twenty micrometer is same as the major length of FOV in the camera, and 20 µm is 1/10 of the length of converging channel at its end (200 µm). So we postulated the RBCs in the ROI behave as if under a constant extensional stress condition and the effect of shear stress is negligible, compared to extensional stress. Roughly, 8% of RBCs passed though the ROI, which was calculated by (Number of RBCs in ROI, x=1,200 µm) / (Number of RBCs in 1,150 µm <×< 1,350 µm) with images from a 10× objective lens. Though it seems to be a low efficient, it is high-throughput way to reduce the experiment time. The micropipette aspiration and optical tweezers method require tremendously time-consuming processes in order to obtain statistically meaningful data, because they require handling the individual cells one by one. Meanwhile, this microfluidic method took less than a minute of acquiring time to obtain the images of more than 1,000 deformed RBCs, when the images were taken with 10 Hz of acquisition rate for Q=10 µl/min.

When the RBC/PVP suspension is introduced into the microchannel with a constant flow rate, before entering the hyperbolic converging region, most RBCs flowing around the center of channel do not deform significantly but maintain their shape (Fig. 3(a)). These cells show a value of almost zero value on the Deformation Index (DI). At the hyperbolic converging region, the RBCs that flow along the centerline elongate and reach the maximum deformation state, they then slowly relax after passing through the converging region.

Since the RBCs maintain a deformed shape while passing through the converging region, we can continuously

take the images of deformed RBCs in the ROI under the constant extensional flow field. Combined with enhanced image by using a band path filter as described in experimental section, the degree of deformation of RBC can easily be quantified by image analysis, and the average and distribution of RBC deformability obtained.

As we increase the extensional stress by increasing input flow rate, more elongated cells are observed (Fig. 3(b) and (c)) and the histogram of frequency (percentage of RBCs) versus DI shifts from low to high DI as expected: average ± standard deviation is 0.42±0.148 under extensional stress of 0.9 Pa, and 0.60±0.106 under extensional stress of 9.0 Pa.

### 3.2 Comparison of deformation under simple shear and extensional flow

Extensional flow is more effective in deformation and break-up of a deformable particle (Dealy and Wissbrun 1990; Barnes 2000). In extensional flow, when a deformable material is suspended in a liquid (e.g. droplet), it stretches and does not undergo rotation while deforming in the flow direction (Fig. 1). Meanwhile in simple shear flow, it rotates and deforms in the shear direction (Dealy and Wissbrun 1990; Barnes 2000) (Fig. 1). This inspired us to investigate the different responses of the RBCs to simple shear and extensional flow.

In order to compare the effect of the flow field on RBC deformation, the average DI value is plotted as a function of the applied stress (Fig. 4). The applied stress was obtained by the correlation: *Applied shear stress = Shear viscosity × Shear rate, Applied extensional stress = Extensional viscosity × Extensional rate.*

In both simple shear and extensional flow, RBCs elongate and the degree of deformation (DI) saturates at a
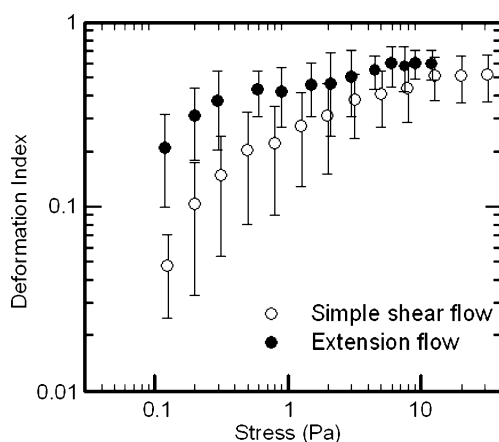


**Fig. 4** Deformation index of RBCs under simple and extensional flow. Each data point was obtained by analysis of more than 500 images and each experiment was repeated three times

high deformation rate. In simple shear flow, the saturated DI is about 0.55 and it occurs at about 20 Pa. In extensional flow, however, the saturated DI is slightly higher and occurs at a lower stress level (about 6 Pa). Thus, at a low stress region before the DI is saturated, the extensional flow is much more efficient in deforming the RBCs than the simple shear flow. Since the range of stress in a human vessel is known to be in between 0.1 Pa and 20 Pa, it is meaningful to consider this result in association with blood circulation or RBC related diseases.

This result points out the limitations of the existing models that predict cell damage, which are based only on shear flow experiments. These models are often used as a guideline for the design of artificial organs. It is apparent that we need to develop more accurate models for better design, because the artificial organs have been pre-evaluated and designed based on these models. They have been used for mechanical damage from high shearing over a short period (instantaneous rupture) (Blackshear and Blackshear 1987; Gierspiepen et al. 1990) or from lower shearing over a long period (leaking).

In the case of instantaneous rupture, a commonly used model is the power-law model: $D = C\tau^\alpha t^\beta$ (where D: damage, $\tau$: shear stress, t: imposed time, and C, $\alpha$, $\beta$: constants). As shown in the model itself, it does not consider the effect of extensional flow. Though it predicts well under the laminar shear flow, there is inconsistency in the complex flow field (Grigioni et al. 2004). Taken into account with the models, our result could help to explain this inconsistency. We suggest that the models should be modified by considering the contribution of the extensional stress to the cell damage.

In the other example, leaking, the RBCs release part of their hemoglobin content into the blood stream through the small reversible openings in the membranes, and the degree of deformation (DI) is closely related to the amount of hemolysis (Arora et al. 2004). The Arora group modified the predictive model to include the contribution of stretching under simple shear flow as follows, $\frac{\Delta Hb}{Hb} = 3.62 \times 10^{-7} \left( \mu_{blood} \sqrt{\frac{f_1^2 DI^2}{(1-DI^2)f_2^2}} \right)^{2.416} t^{0.785}$, ($f_1$, $f_2$: constant, $\mu_{blood}$: blood viscosity, Hb: hemoglobin in plasma). According to this equation, the degree of deformation is one of the dominant parameters of cell damage. By considering the deformation under extensional flow and performing more experiments under the mixed flow field, we expect to improve models in order to predict the blood damage more accurately. This will be critical in developing better artificial organs.

Additionally, we tried to apply this device to the mechanically damaged-RBCs. Unfortunately, instantaneous rupture cannot be observed using this device because leaking of the microfluidic device occurred at high flow

rate of viscous PVP solution (around 50 μL/min). We are still attempting to design a platform for visualizing instantaneous rupture under extensional flow. However, we could observe the difference of deformability between normal and mechanically induced subhemolytic damaged RBC (Data not shown here).

### 3.3 Diagnostic method: detecting the change of RBC deformability

We investigated the deformation of hardened RBCs under the extensional flow field. The change of deformability has been studied to diagnose or predict estimate several specific diseases. Heat treatment is typically known to increase the membrane elasticity with only a slight effect on membrane viscosity (Fisher et al. 1992). We incubated suspensions of RBCs at 45°C for 0 min to 40 min to gradually reduce the cell deformability. Table 1 shows that we can detect the difference of RBC deformability change with high precision. Statistical analysis was performed by Student's $t$ test and ANOVA. The p values obtained from the test were used to estimate the statistical significance of the difference. This difference was found to be statistically significant ($p<0.001$) at every extensional stress level when we compared every pairs of heat treatment duration (incubation time): 0 min and 20 min, 0 min and 40 min, 20 min and 40 min. A histogram of the deformation index (DI) (Extensional stress=3.0 Pa) shows a clear difference and the existence of less deformable RBCs (ex. DI<0.35) in cases of heat treatment for 20 min and 40 min (Fig. 5).

In addition, the opportunity to accurately detect the impairment of RBC deformability by the extensional properties—deformability and its distribution under extensional flow—may provide useful information on the cell behavior as they pass through extension dominant regions as in catheter and phlebotomy needles. When a cell tries to pass through the capillary from a relatively large microvessel, the RBC deformability, not only in shear but also in extensional flow, may determine whether it able to pass. The less deformable cells may block the capillary or cause ischemia in the tissue. The fraction of less deformable
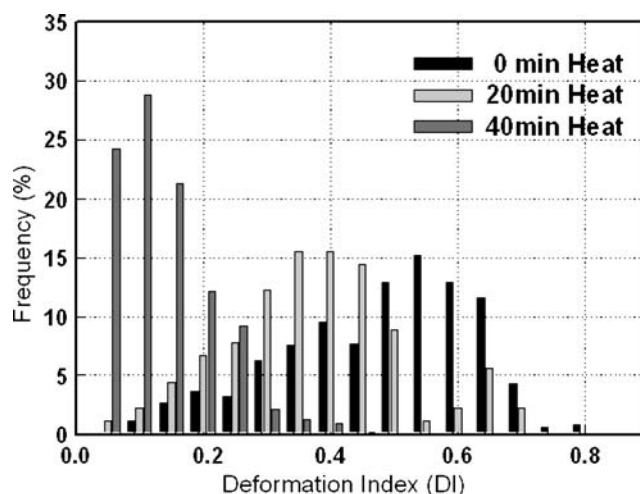


Fig. 5 Distribution of RBC deformability under 3.0 Pa of extensional stress. The RBC/PVP suspension was incubated at 45°C during 0 min, 20 min and 40 min, respectively and each experiment was repeated three times

RBCs is important in this regard, but is hard to obtain using the conventional methods such as micropipet and optical tweezers due to time consuming processes. Our method, which can provide the information about the fraction of less deformable cells, is expected to overcome the limitation of the previous methods and provide a promising way to study the clinical meaning of RBC deformability.

## 4 Conclusion

We proposed a new approach to assess RBC deformability and its distribution under the extensional flow field using a hyperbolic converging microchannel with image enhancement. The results confirm that the extensional flow is much more efficient in cell deformation. As it is able to detect the heat-induced impairment of RBC deformability, this experiment can be applied to detect and diagnose several diseases related to RBC deformability with a small amount of blood and a short period of time. Also this method is expected to provide insights for the better design of circulatory prosthetic devices such artificial valves and pumps.

Table 1 Change of deformation index (DI) according to the heat-treatment time incubated at 45°C

| Extensional stress (Pa) | DI w/ heat treatment for 0min | DI w/ heat treatment for 20min | DI w/ heat treatment for 40min |
|---|---|---|---|
| 0.9 | 0.42±0.148 | 0.25±0.135 | 0.14±0.067 |
| 1.5 | 0.46±0.149 | 0.36±0.138 | 0.21±0.056 |
| 3.0 | 0.51±0.198 | 0.43±0.165 | 0.27±0.154 |
| 6.0 | 0.60±0.147 | 0.46±0.181 | 0.29±0.207 |

The values represent average ± standard deviation. Significant decrease was observed at 20 min and 40 min of heat treatment compared to the standard sample (no heat treatment: 0 min). The p values obtained by Student's $t$-test and were below 0.001 for every extensional stresses when compared each pairs of heat treatment duration: 0 min and 20 min, 0 min and 40 min, 20 min and 40 min

## References

D. Arora, M. Behr, M. Pasquali, Artif. Organs **28**, 1002 (2004)

H.A. Barnes, *A handbook of elementary rheology* (The University of Wales Institute of Non-Newtonian Fluid Mechanics, Wales, 2000), pp. 151–163

P.L. Blackshear, G.L. Blackshear, *Handbook of bioengineering* (McGraw-Hill, New York, 1987), pp. 15.1–15.19

M.C. Dao, T. Lim, S. Suresh, J. Mech. Phys. Solids **51**, 2259 (2003)

J.M. Dealy, K.F. Wissbrun, *Melt rheology and its role in plastics processing* (Nostrand Reinhold, New York, 1990), pp. 231–268

V. Delinder, A. Groisman, Anal. Chem. **78**, 3765 (2006)

J.G. Dobbe, G.J. Streekstra, M.R. Hardeman, C. Ince, C. Grimbergen, Cytometry **50**, 313 (2002)

E. Evans, Biophys. J. **43**, 27 (1983)

F. Feigl, F.X. Tanner, B.J. Edwards, J.R. Collier, J. Non-Newtonian Fluid Mech. **115**, 191 (2003)

M.T. Fisher, R.B. Wenby, H.J. Meiselman, Biorheology **29**, 185 (1992)

M. Gierspiepen, L.J. Wurzinger, R. Opitz, H. Reul, Int. J. Artif Organs **13**, 300 (1990)

M.S. Grant, J. Emerg. Nurs. **29**, 116 (2003)

M. Grigioni, C. Daiele, U. Morbiducci, G. D'avenio, G. Benedetto, V. Barbaro, Artif. Organs **28**, 467 (2004)

D.S. Kim, S.H. Lee, C.H. Ahn, J.Y. Lee, T.H. Kwon, Labchip **6**, 794 (2006)

C. Mobuchon, P.J. Carreau, M. Heuzey, M. Sepehr, Polym. Compos. **26**, 247 (2005)

F.C. Mokken, M. Kedaria, C.P. Henny, M.R. Hardeman, A.A. Gelb, Ann. Hematol. **64**, 113 (1992)

M. Paulitschke, G.B. Nash, Clin. Hemorheol. Microcirc. **13**, 407 (1993)

G.C. Randall, K.M. Schultz, P.S. Doyle, Labchip **6**, 516 (2006)

M.K. Sharp, S.F. Mohammad, Ann. Biomed. Eng. **26**, 788 (1998)

S. Simchon, K.M. Jan, S. Chien, Am. J. Physiol. **253**, 893 (1987)

R. Suwanarusk, B.M. Cooke, A.M. Dondorp, K. Silamut, J. Sattabongkot, N.J. White, R. Udomsangpetch, J. Infect. Dis. **189**, 190 (2004)

F.T. Trouton, Proc. Royal Soc. **77A**, 426–440 (1906)

M. Umezu, Proceedings of the ASME International Mechanical Engineering Congress and Exposition (ASME advances in bioengineering). **28**, 33 (1994)

Y.N. Xia, G.M. Whitesides, Angew. Chem. Int. Edit. **37**, 551 (1998)

S. Yang, A. Undar, J.D. Zahn, Labchip. **6**, 871–880 (2006)